Tribology International 188 (2023) 108772

Contents lists available at ScienceDirect

Tribology International

journal homepage: www.elsevier.com/locate/triboint

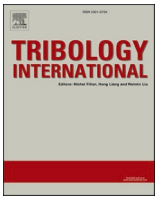

Effect of rolling on fretting fatigue assessment of cylindrical contact in partial slip regime

Sabrina Vantadori [a,*], Andrea Zanichelli [a], Diego Erena [b], Jesús Vázquez [b]

[a] Department of Engineering & Architecture, University of Parma, Parco Area delle Scienze 181/A, 43124 Parma, Italy
[b] Universidad de Sevilla, Escuela Técnica Superior de Ingenieros, Departamento de Ingeniería Mecánica y Fabricación, Camino de los Descubrimientos s/n, C.P., 41092, Spain

ARTICLE INFO

Keywords:
Crack path
Fretting fatigue
Fatigue lifetime
Rolling

ABSTRACT

The present research work deals with the fatigue assessment of an Al 7075-T651 subjected to fretting fatigue testing characterised by cylindrical contact. A small rolling of the pads is experimentally observed and, consequently, the contact surface stresses are different to the hertzian one. Therefore, the methodology, recently proposed by some of the present authors for the fatigue assessment of fretting-affected metallic components, is here employed for the first time in conjunction with a FE numerical model able to take into account the effect of the rolling of the pads, in order to find out both the crack nucleation orientation and the lifetime for each specimen of the experimental campaign analysed.

1. Introduction

Nowadays, a high variety of metallic structural components, such as running cables and overhead conductors, shrink-fitted shafts, spline coupling, dovetail joints, bolt and riveted joints, fuel rods cladding and steam generator tubes of nuclear power plants, are still subjected to failures due to fretting fatigue, thus resulting in catastrophic events [1–7].

In such a context, where high stress-gradients arise near the contact zone [8,9], specific studies have been aimed to determine the stress field within the components in contact, by employing both analytical and numerical tools.

Relatively to the analytical tools, Hertz [10] firstly studied the case of frictionless contact between two homogeneous linear-elastic half-spaces in presence of a constant normal load. Under the assumptions that the elasticity theory holds and the contact area is very small with respect to the size and radii of curvature of the bodies in contact, such a solution can be applied to any pair of either spherical or cylindrical shaped bodies characterised by different radii of curvature.

Starting from the hertzian solution, many researchers proposed analytical closed-form solutions related to different fretting fatigue conditions. Cattaneo [11] and Mindlin [12] considered the presence of a tangential load in addition to the constant normal load generating a partial slip condition that is, the case of the contact area partialisation into an outermost zone (where relative surface micro-slips occur) and an innermost zone (where no relative motion takes place between the two bodies).

This latter solution was subsequently extended to the case of a bulk cyclic load acting on one of the two bodies in contact [13], causing the shift of the inner stick region. Moreover, Vázquez et al. [14] studied the case of a high value of the applied bulk load, determining two distinct outer slip zones where micro-slips of opposite sign occurred. Other attempts have been done to extend the above solutions, for instance, to more general geometries [15] and problems characterised by varying normal load [16].

Another approach to the fretting fatigue problem was provided by the asymptotic analysis, according to which the stress concentration due to the contact is considered analogously to cracks in fracture mechanics. Such an approach has been mainly employed to analyse conditions where the hertzian theory fails. The case of complete contact problems characterised by sharp contact edges, for instance, was studied by Williams [17] and Bogy [18]. Moreover, Dini and Hills [19] analysed the fretting fatigue condition in partial slip regime, providing a comparison with the results obtained by employing the abovementioned Cattaneo-Mindlin solution, whereas Fleury et al. [20] considered more complex loading histories.

Relatively to the numerical tools, many efforts have been made by the researchers in recent decades in order to cover all the situations where the assumptions of the analytical theories are violated. In such a

* Corresponding author.
E-mail address: sabrina.vantadori@unipr.it (S. Vantadori).

https://doi.org/10.1016/j.triboint.2023.108772
Received 29 May 2023; Received in revised form 27 June 2023; Accepted 5 July 2023
Available online 7 July 2023

Nomenclature

a_H	theoretical hertzian contact half-width.
a_R	average experimental value of the contact half-width.
C_a	amplitude of the stress component lying on the critical plane.
d	average grain size of the material.
E	elastic modulus.
E^*	elastic modulus for plain strain condition.
H_{cal}	estimated crack nucleation location (hot-spot).
H_{exp}	experimental crack nucleation location.
m	slope of the S-N curve under fully reversed normal loading.
m^*	slope of the S-N curve under fully reversed shear loading.
N_a	amplitude of the stress component normal to the critical plane.
N_{cal}	number of loading cycles to failure estimated neglecting the rolling of the pads in the FE model.
N_{cal}^R	number of loading cycles to failure estimated incorporating the rolling of the pads in the FE model.
$N_{eq,a}$	equivalent normal stress amplitude.
N_{exp}	experimental number of loading cycles to failure.
N_m	mean value of the stress component normal to the critical plane.
$\bar{N}_a$	average value of N_a.
$\bar{N}_m$	average value of N_m.
P	constant normal force applied to the pads.
$Q(t)$	cyclic tangential force applied to the pads.
Q_a	amplitude of the cyclic tangential force.
R	radius of the pads.
t	time.
S_{cr}	verification point.
α	orientation of the critical plane candidate.
α_{cal}	crack nucleation orientation estimated neglecting the rolling of the pads in the FE model.
α_{cal}^R	crack nucleation orientation estimated incorporating the rolling of the pads in the FE model.
α_{exp}	experimental crack orientation.
f	friction coefficient.
ν	Poisson coefficient.
$\theta(t)$	cyclic rotation of the pads.
θ_{max}	maximum value of rotation of the pads.
$\sigma_{af,-1}$	material fatigue strength under fully reversed normal loading, at a reference number N_0 of loading cycles.
$\sigma_B(t)$	cyclic axial stress applied to the specimen.
$\sigma_{B,a}$	amplitude of the cyclic axial stress.
σ_u	ultimate tensile strength.
$\tau_{af,-1}$	material fatigue strength under fully reversed shear loading, at a reference number N_0 of loading cycles.

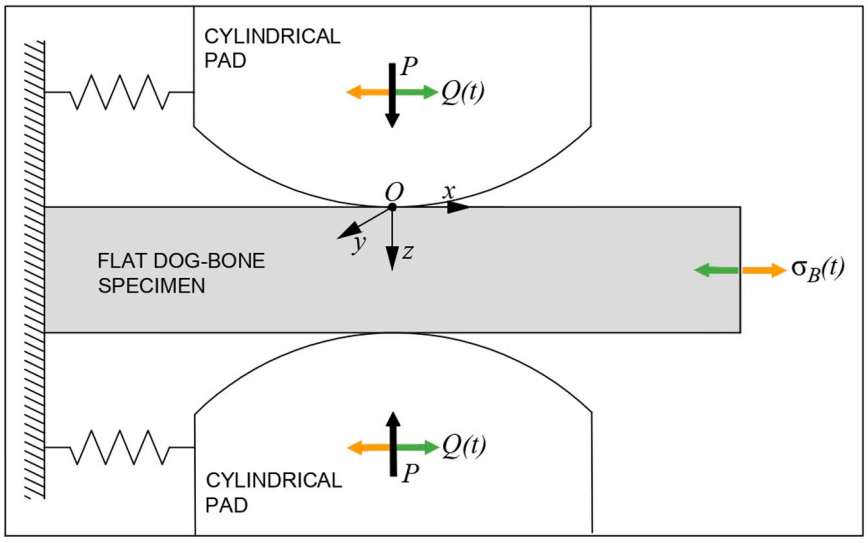

Fig. 1. Schematisation of the contact problem analysed.

context, the Finite Element (FE) method has been largely employed, providing satisfactory results in analysing fretting fatigue problems characterised by complex geometry and loading history, presence of voids in the material and specific physical phenomena (i.e., rolling, debris formation, mass-eccentricity) that could not be considered by the theoretical formulations for reasons of simplicity and generality of the solution [21–29]. Moreover, FE models have been developed in order to consider the effect of wear [30] or to overcome the limitations of an elastic analysis by including plasticity [31].

Further, the extended FE method has recently provided the opportunity to enrich the solution of standard FE method, by implementing discontinuous functions. Moës et al. [32] developed an extended FE model to simulate, without any remeshing, the fatigue crack growth. In order to estimate the stress intensity factors in complete contact problems by employing a coarse mesh in favour of a low computational effort, Giner et al. [33] enriched the FE formulation by employing singular expressions. Moreover, Cardoso et al. [34] have used enrichment functions to achieve accurate contact stress solutions even when using coarse meshes.

Recently, some of the present authors have proposed a methodology for the fatigue assessment of fretting-affected metallic structures [35–38]. According to such a methodology, whose peculiarity is also to incorporate a material microstructure-related parameter, the fretting fatigue assessment is performed through the multiaxial fatigue criterion by Carpinteri et al. [39–42], employed in conjunction with the Critical Direction Method [43,44].

Table 1
Mechanical [45] and fatigue [47] properties of the Al 7050-T651 aluminium alloy examined.

Material	$E[GPa]$	$\nu[-]$	$\sigma_u[MPa]$	$\sigma_y[MPa]$	$\sigma_{af,-1}[MPa]$	$m[-]$	$\tau_{af,-1}[MPa]$	$m^*[-]$	$N_0[cycles]$
Al 7050-T651	71	0.33	572	503	193	-0.12	111	-0.12	$2{\cdot}10^6$

Table 2
Fretting loading conditions applied (P, Q_a and $\sigma_{B,a}$), theoretical and experimental contact half-width (a_H and a_R), and experimental both crack nucleation location (x_{exp}), crack orientation (α_{exp}) and fatigue life (N_{exp}).

Test No.	$P[N/mm]$	$Q_a[N/mm]$	$\sigma_{B,a}[MPa]$	$a_R[mm]$	$a_H[mm]$	$x_{exp}[mm]$	$\alpha_{exp}[^\circ]$		$N_{exp}[cycles]$
							$\mu[^\circ]$	$\sigma[^\circ]$	
T1	527	193	110	1.64	1.30	1.41	32.0	13.9	88216
T2									89376
T3	679	121	150	1.74	1.47	1.54	15.9	4.5	47737
T4									51574
T5	679	193	150	1.80	1.47	1.48	28.5	7.5	50268
T6									39202

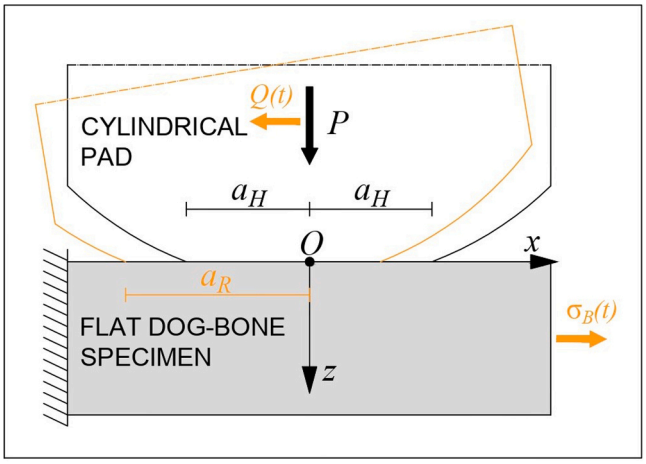

Fig. 2. Schematisation of the rolling phenomenon (only one pad is represented in the Figure).

In the present research work, the abovementioned methodology is employed for the first time, together with the FE numerical model recently proposed by Erena et al. [23,45], for the analysis of the fretting fatigue tests presented in Ref. [46], characterised by a cylindrical contact and rolling of the contact pads. Both a FE model neglecting and a FE model incorporating the rolling of the pads are considered. Subsequently, by exploiting the stress field coming from the above FE analyses, the methodology for fretting fatigue assessment is employed in order to determine both the crack nucleation orientation and the fatigue life of the tested specimens.

2. Experimental fretting tests analysed

The experimental campaign carried out by some of the present authors [46] at the University of Seville is analysed in the present paper. In particular, fretting fatigue tests were performed in partial slip regime. The testing setup consisted in two pads, characterised by a cylindrical shape of the contact surface with a radius, R, equal to 100 mm, placed in contact with a flat specimen, characterised by a dog-bone shape with a rectangular cross section in the central part (being the width equal to 10 mm, whereas the thickness equal to 8 mm). The schematisation of the contact problem involving both pads and specimen is shown in Fig. 1.

Both specimens and pads were made of Al 7050-T651 aluminium alloy, which is widely employed due to its high strength-to-weight ratio in a variety of applications where catastrophic fretting fatigue failures still occur (such as aircraft structural components, gears, fuse parts, connections, highly stressed parts, and structural components used in the automotive and aerospace industries). Such an alloy is characterised by the mechanical [45] and fatigue [47] properties that have been listed in Table 1, an average grain size, d, equal to 50μm [45] and a coefficient of friction, f, of 0.75 (in a cylindrical contact configuration) [46].

Three different fretting loading conditions were examined, as listed in Table 2. During each test, a constant normal force, P, was firstly applied to the pads, in order to push them against the specimen, as schematically shown in Fig. 1. Subsequently, a cyclic axial stress, $\sigma_B(t)$ (loading ratio equal to -1), was imposed on the specimen, with a frequency equal to 10 Hz (Fig. 1). Consequently, due to the compliance of the fretting device, a cyclic tangential load, $Q(t)$ (in phase with the cyclic axial stress), arose in the pads with opposite direction with respect to $\sigma_B(t)$ (see Fig. 1). The amplitude, Q_a, of such a tangential load depended on the amplitude, $\sigma_{B,a}$, of the axial stress applied on the specimen, and could be adjusted by modifying the stiffness of the adjustable supports of the pads. Details may be found in Ref. [46]. The experimental number of loading cycles to failure, N_{exp}, is listed in Table 2 for each tested specimen.

The contact zone was measured in correspondence of the fretting scars by means of an optical microscope. Then, such images were analysed through a CAD software to compute the average value of the contact half-width, a_R, listed in Table 2. More details related to such a procedure can be found in Ref. [45]. It was observed that, for each loading condition analysed, the value of a_R was significantly higher than the theoretical hertzian contact half-width, a_H, given by:

$$a_H = \sqrt{\frac{4PR}{\pi E^*}} \tag{1}$$

As it is proved in Ref. [23], this was the result of the rolling phenomenon, that is, due to the stiffness of the supports, when the cyclic axial stress was imposed on the specimen, the pads experienced a rotation that promoted the contact zone to move in the direction opposite to that of the cyclic axial load applied (see Fig. 2). In other words, if an entire loading cycle was considered, although the contact width was instantaneously equal to 2 a_H, the overall observable contact width (i.e., the width of the scars at the end of the cycle) was greater than 2 a_H and equal to 2 a_R. The maximum value of the above rotation, θ_{max}, was computed by employing the pad radius and the arc length of the pad surface that came into contact due to rolling, obtained as $a_R - a_H$ [23]. Such a maximum value was equal to 0.19° for tests No. T1, T2, T5 and T6, and 0.15° for tests No. T3 and T4.

Moreover, the crack nucleation location on the contact surface, H_{exp}, was found by employing the abovementioned procedure described for

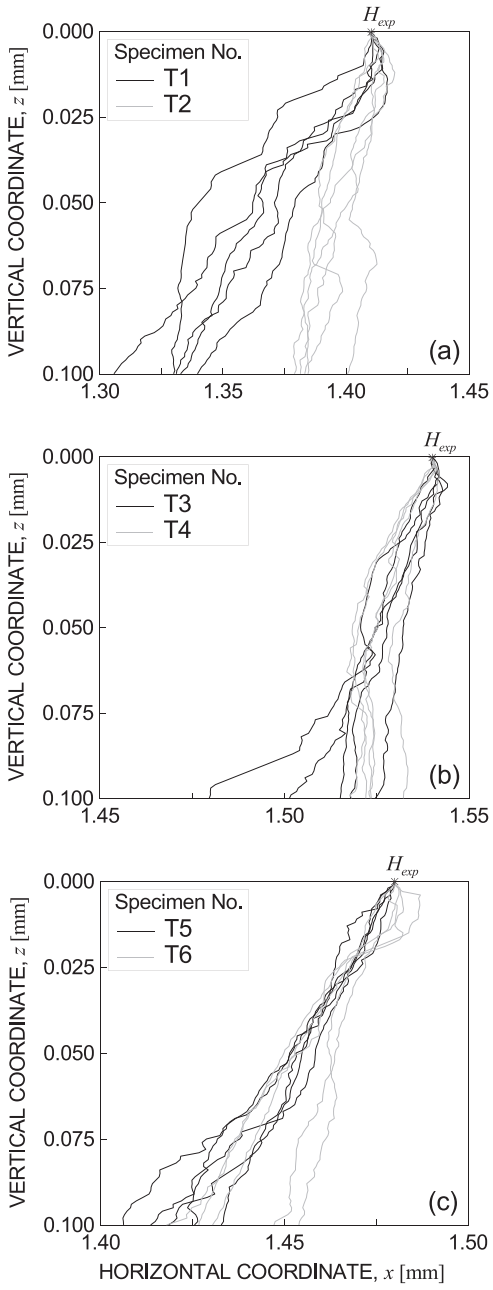

Fig. 3. Experimental crack profiles related to the tests No.: (a) T1-T2, (b) T3-T4, and (c) T5-T6.

the contact width determination. More precisely, an average value x_{exp} (see the reference system shown in Fig. 1) of the crack nucleation location was obtained for each tested specimen. The average crack nucleation location experimentally observed, x_{exp}, is listed in Table 2 for each loading condition.

Furthermore, in order to analyse the crack profiles experimentally observed, a three-dimensional map of the crack surface was obtained through a confocal microscope for each tested specimen [45]. Subsequently, from such 3D maps, different experimental crack profiles were extracted for each specimen analysed and reported in Fig. 3.

The cracks were observed to be characterised by an experimental crack orientation, α_{exp}, equal to 13° and 39° for the tests No. T1 and T2, 9° and 18° for the tests No. T3 and T4, and 24° and 31° for the tests No. T5 and T6. Note that such values have been obtained by linearly interpolating each experimental crack profile up to 100 μm depth. The angle measured from the obtained line and the line perpendicular to the material surface has been assumed as α_{exp}. The mean values, μ, and corresponding standard deviations, σ, of the experimental crack orientation, α_{exp}, are listed in Table 2.

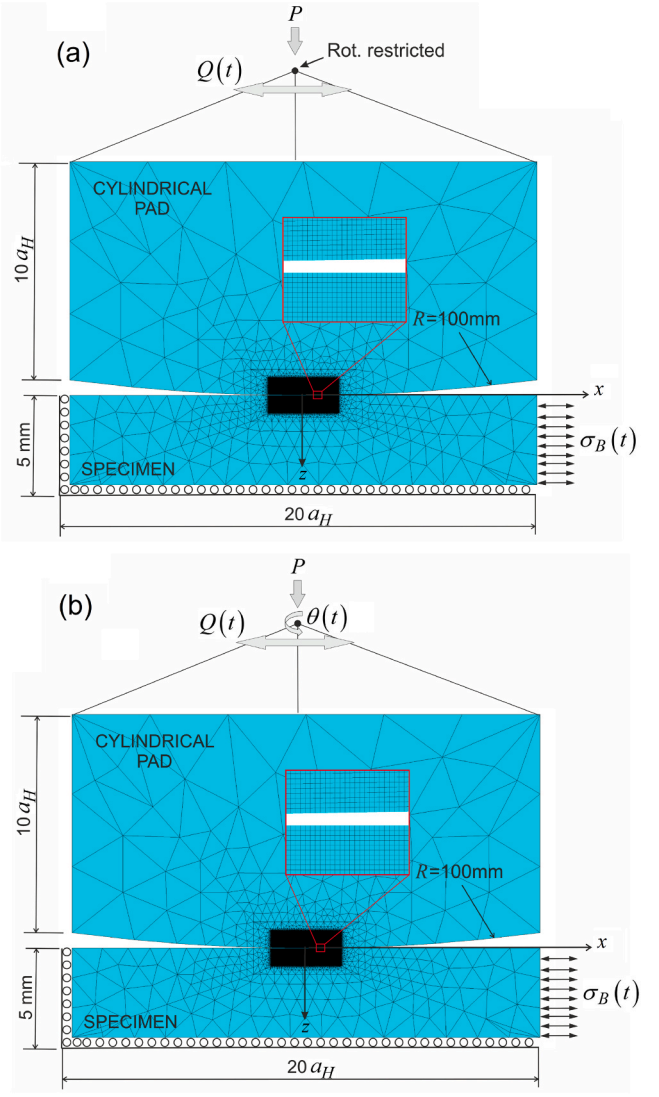

Fig. 4. FE models employed: (a) neglecting and (b) incorporating the rolling of the pad.

3. FE numerical models employed

The FE numerical models, employed for the analysis of the fretting fatigue tests summarised in **Section 2** , are hereafter described. In particular, a FE model that neglects the rolling of the pads and a FE model that incorporates its effect (both of them recently proposed by Erena et al. [23,45]) are employed in the present work for the determination of the stress field in the tested specimens.

3.1. Numerical model neglecting rolling

A FE numerical model has been recently proposed by Erena et al. [23,45] for the analysis of fretting fatigue tests characterised by cylindrical contact. In particular, by employing such a model, the experimental campaign described in **Section 2** may be simulated by neglecting the rolling of the pads.

The commercial software ANSYS® is employed for the numerical simulations. As shown in Fig. 4 **(a)**, only half a specimen is considered

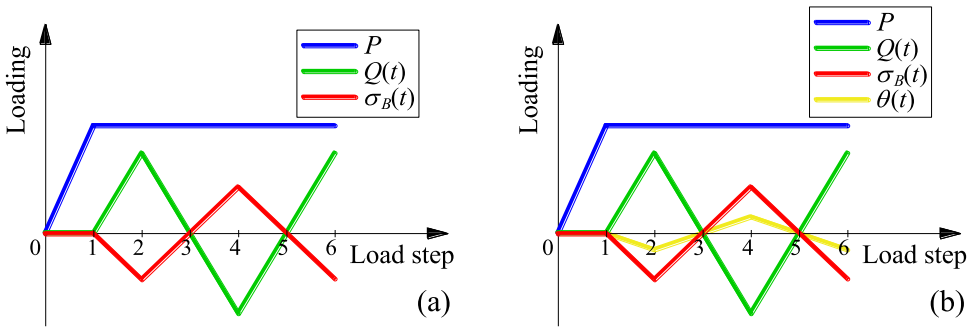

Fig. 5. Loading histories applied in FE models: (a) neglecting and (b) incorporating the rolling of the pad.

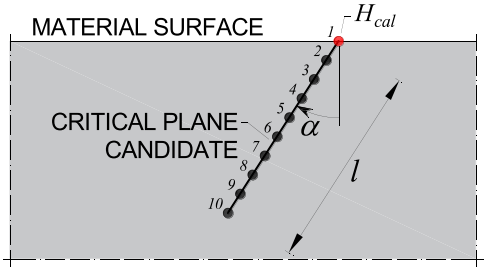

Fig. 6. Scheme for determining the critical plane orientation. Positive values of α are considered when the segment is towards the centre of the contact zone.

and the contact with one of the two fretting pads is modelled, since the contact problem analysed is characterised by a symmetry condition. The boundary conditions used to reproduce the testing setup are shown in the same figure too.

A constant normal force and a cyclic tangential force are applied to a master node (the rotation of such a node is restricted), which is able to distribute such loading conditions to all the nodes that are located at the top of the pad, whereas a cyclic axial stress is directly applied to the specimen. The constant normal force, P, is applied in the first load step in order to bring the specimen and the pad into contact. Subsequently, $Q(t)$ and $\sigma_B(t)$ are simultaneously applied with opposite directions and made to vary, while P is kept constant. Each load is applied by means of small increments according to the loading history shown in Fig. 5 (a). Note that, in the load step No. 4 the maximum value of $\sigma_B(t)$ is applied to the specimen, whereas the minimum one is attained in the load steps No. 2 and 6.

A plane strain condition is assumed in the numerical model, due to the values of both the pad/specimen thickness and the contact length. Therefore, 2D plane linear elements, named PLANE182, characterised by two degrees of freedom at each node, are used with triangular or quadrilateral shape in both the specimen and the pad. A total number of 315000 finite elements has been used. In order to accurately capture the high stress/strain gradient due to the contact problem, a very refined mesh is defined after a convergence analysis at the contact interface, with 5 μm-size quadrilateral elements. Moreover, CONTA171 and TARGE169 elements are used to model the contact pair on the specimen and pad surfaces, respectively. In this region of the model, the augmented Lagrangian algorithm is set for the contact, and a Coulomb friction law is used with a coefficient of friction equal to 0.75.

The default values for the normal, FKN, and tangential, FKT, stiffness factors and for the slip tolerance factor, SLTO, are assumed.

3.2. Numerical model incorporating rolling

A FE numerical model has been recently proposed by Erena et al. [23,45] for the analysis of fretting fatigue tests characterised by cylindrical contact, by also taking into account the rolling of the pads. In particular, by employing such a model, the experimental campaign described in **Section 2** may be simulated incorporating the rolling of the pads.

The commercial software ANSYS® is employed for the numerical simulations. As shown in Fig. 4 (b), only a half of the specimen and one pad are considered in the model due to symmetry condition. The boundary conditions used to reproduce the testing setup are shown in the same Figure too.

A constant normal force, a cyclic tangential force and a cyclic in-plane rotation are applied to a master node, which is able to transfer them to all the nodes that are located at the top of the pad, whereas a cyclic axial stress is directly applied to the specimen. The constant normal force, P, is applied in the first load step in order to bring the specimen and the pad into contact. Subsequently, the cyclic tangential force, $Q(t)$, the cyclic in-plane rotation, $\theta(t)$, and the cyclic axial stress, $\sigma_B(t)$, are simultaneously applied and made to vary, while P is kept constant, according to the loading history shown in Fig. 5 (b). Note that, in the load step No. 4 the maximum tensile stress is achieved in the specimen, whereas both a tangential load (acting in the direction corresponding to $-x$) and a counter clockwise rotation are applied to the master node.

The maximum value for the cyclic in-plane rotation, used in the present numerical model incorporating rolling, was computed as the average value of the maximum rotation experimentally observed for each loading condition (see Section 2), that is 0.19° for the simulations of the tests No. T1, T2, T5 and T6, and 0.15° for that of the tests No. T3-T4.

The element types, contact formulation and parameters are the same described in Section 3.1.

4. Methodology for fretting fatigue assessment

The methodology here applied for the fatigue assessment of fretting-affected metallic structures [35–38] needs some *input data*. More in detail, it is necessary to know:

- the geometric sizes of the bodies in contact (i.e., the specimen and the pads);
- the loading and the boundary conditions of the contact problem;
- the material mechanical properties (for both the specimen and the pads), that is, the elastic modulus, E, the Poisson coefficient, ν, and the ultimate tensile strength, σ_u;
- the material fatigue properties for the specimen, that is, both the fatigue strengths, $\sigma_{af,-1}$ and $\tau_{af,-1}$, and the slope of the S-N curve, m and m^*, under fully reversed normal and shear loading, respectively, at a reference number N_0 of loading cycles;
- the material average grain size, d, for the specimen;
- the coefficient of friction, f, between the specimen and the pads.

First of all, the *stress field* in the specimen needs to be computed. In the present research work, the FE numerical models described in **Section 3** are used to this aim.

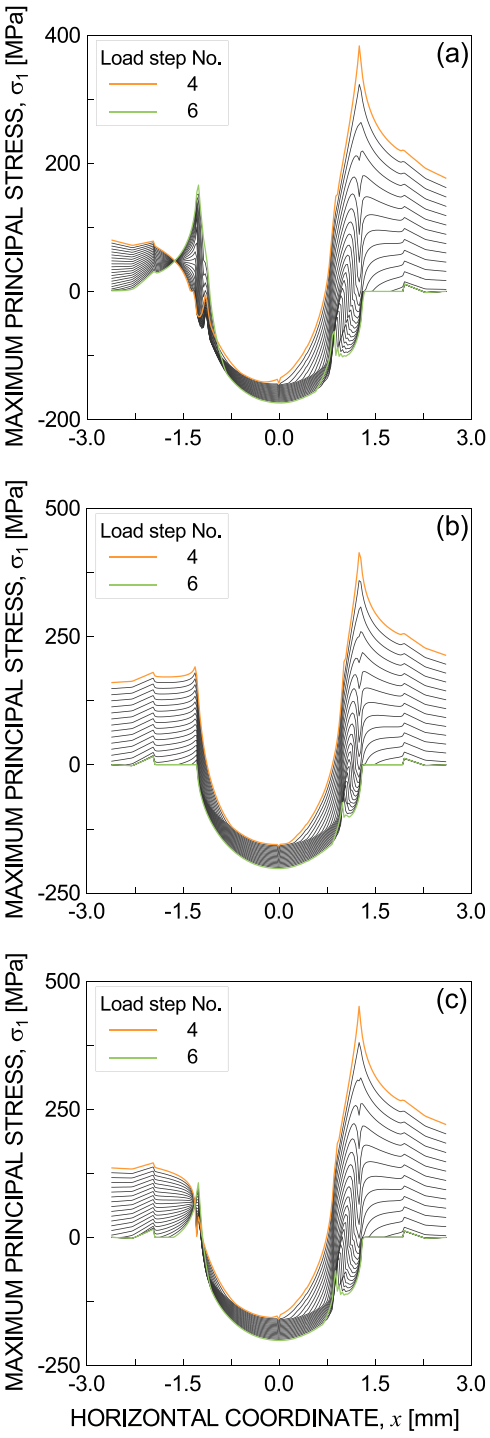

Fig. 7. Maximum principal stress, σ_1, along the contact surface, obtained with the FE model neglecting rolling at different time steps between the load steps No. 4 and 6 (see Fig. 5(a)), for the loading conditions of the tests No.: (a) T1-T2, (b) T3-T4, and (c) T5-T6.

Subsequently, the *crack nucleation location*, H_{cal}, (that is, the hot-spot location on the material surface) is found: it is the point on the material surface achieving the maximum value of σ_1 in one fretting cycle, being σ_1 the maximum among the principal stresses.

Subsequently, the *crack nucleation orientation* is determined. This orientation is assumed to coincide with that of the critical plane, α_{cr}, which is found according to the Critical Direction Method (CDM) proposed by Araujo et al. [43,44]. By assuming a plane strain condition for the considered contact problem, each critical plane candidate appears as

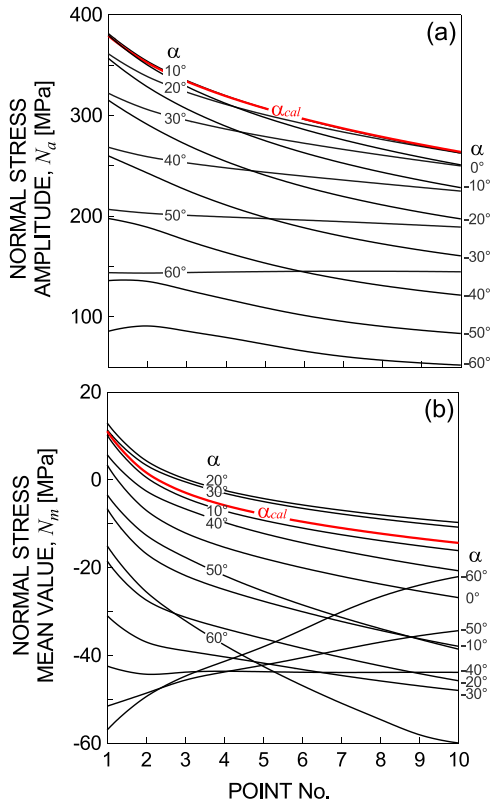

Fig. 8. Tests No. T1-T2: (a) amplitude and (b) mean value of the normal stress component computed in equally-spaced points along each α – oriented segment, from the hot-spot (point 1) up to $2d$ (point 10), by neglecting the rolling of the pad.

a segment of given length, l, which starts from H_{cal}, as shown in Fig. 6. According to the present methodology, the physical size l is assumed equal to $2d$. Moreover, the orientation, α, of such a segment is identified as shown in Fig. 6.

A fatigue parameter is computed for each segment obtained by varying α ($-90° \leq \alpha \leq +90°$ and $\Delta\alpha$=1°). The orientation identifying the maximum value of the fatigue parameter is considered as that corresponding to the critical plane one, α_{cr}.

According to the present methodology, the fatigue parameter is $N_{eq,a}$, and it is given by [39–42]:

$$N_{eq,a} = \bar{N}_a + \sigma_{af,-1}\left(\frac{\bar{N}_m}{\sigma_u}\right) \tag{2}$$

being $\bar{N}_a$ and $\bar{N}_m$ the average values, computed for each α – oriented segment, of the amplitude, N_a, and of the mean value, N_m, of the normal stress component perpendicular to the critical plane candidate. Note that, N_a and N_m are computed in many equally-spaced points along each critical plane candidate, from the hot-spot up to $2d$ (see Fig. 6).

Finally, the *fatigue life*, N_{cal}, is estimated according to the Carpinteri et al. criterion [39–42], by employing the stress components acting on the critical plane at the verification point, S_{cr}, located at a distance $2d$ from the hot-spot along a segment with an orientation α_{cr}, by employing the following equation:

$$\sqrt{\left[N_a(2d,\alpha_{cr}) + \sigma_{af,-1}\left(\frac{N_m(2d,\alpha_{cr})}{\sigma_u}\right)\right]^2 + \left(\frac{\sigma'_{af,-1}}{\tau'_{af,-1}}\right)^2 [C_a(2d,\alpha_{cr})]^2} = \sigma'_{af,-1} \tag{3}$$

where C_a is the amplitude of the shear stress component lying on the critical plane, and $\sigma'_{af,-1}$ and $\tau'_{af,-1}$ are given by:

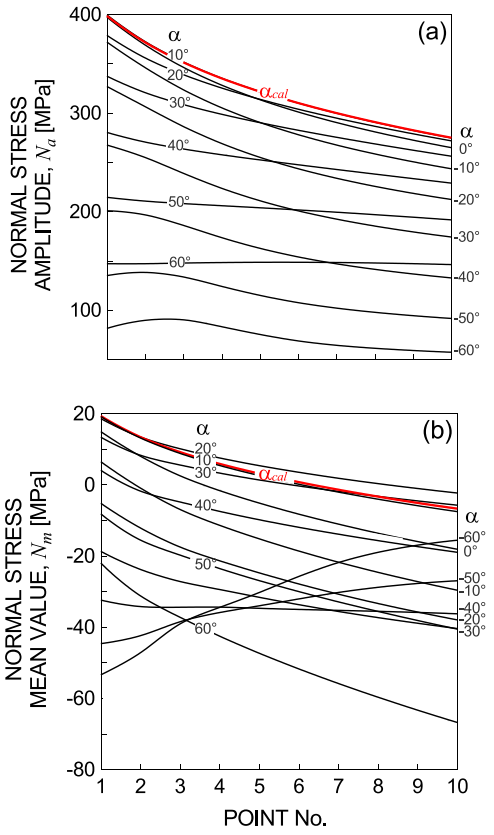

Fig. 9. Tests No. T3-T4: (a) amplitude and (b) mean value of the normal stress component computed in equally-spaced points along each α – oriented segment, from the hot-spot (point 1) up to 2d (point 10), by neglecting the rolling of the pad.

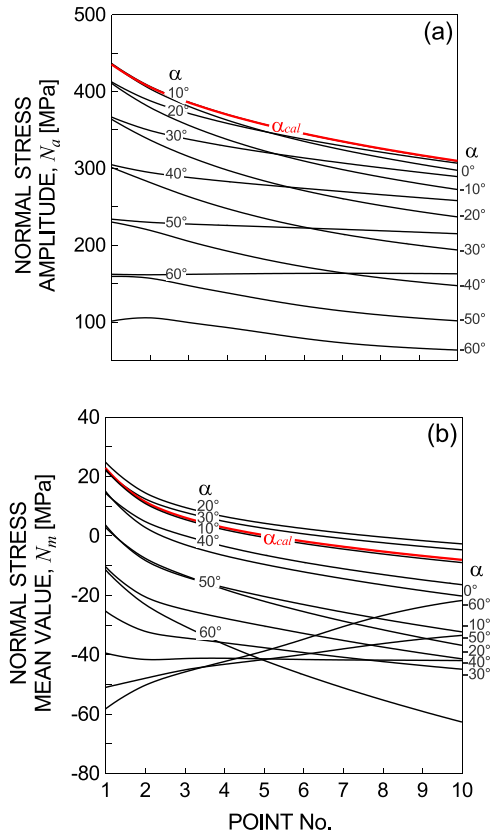

Fig. 10. Tests No. T5-T6: (a) amplitude and (b) mean value of the normal stress component computed in equally-spaced points along each α – oriented segment, from the hot-spot (point 1) up to 2d (point 10), by neglecting the rolling of the pad.

$$\sigma'_{af,-1} = \sigma_{af,-1}\left(\frac{N_{cal}}{N_0}\right)^{m} \tag{4a}$$

$$\tau'_{af,-1} = \tau_{af,-1}\left(\frac{N_{cal}}{N_0}\right)^{m^*} \tag{4b}$$

5. Results and discussion

The experimental campaign described in Section 2, is herein analysed by employing the methodology for fretting fatigue assessment summarised in Section 4, where the stress state which serves as an input for this methodology is determined through the FE numerical models described in Section 3. In particular, the results obtained without considering the rolling of the pads (that is, by employing the FE numerical model described in sub-Section 3.1) are reported in sub-Section 5.1, whereas sub-Section 5.2 is devoted to the results obtained by taking into account the effect of rolling (that is, by employing the FE numerical model described in sub-Section 3.2).

5.1. Results obtained neglecting rolling

Firstly, the hot-spot, H_{cal}, is determined. In particular, such a point is found at $x_{cal} = 1.25mm$, $1.42mm$, and $1.42mm$ for the simulations of the tests No. T1-T2, T3-T4, and T5-T6, respectively. In particular, it can be noted that the hot-spot is found inside the slip zone for all the simulations performed, in agreement with the experimental results. By considering the loading conditions of the tests No. T1-T2, T3-T4 and T5-T6, the maximum principal stress, σ_1, along the contact surface is plotted in Fig. 7(a), (b) and (c), respectively, for 14 different equally-spaced time steps between the load steps No. 4 and 6 (see Fig. 5**(a)**).

Subsequently, the crack nucleation orientation, α_{cal}, is determined for each loading condition analysed. N_a and N_m are computed in 10 equally-spaced points along each α – oriented segment (see Fig. 6), from the hot-spot (point 1) up to 2d (point 10). Such values are plotted in Figs. 8–10 for the loading conditions of the tests No. T1-T2, T3-T4 and T5-T6, respectively.

Then, the average values, $\bar{N}_a$ and $\bar{N}_m$, of the above stress components are determined, in order to compute the fatigue parameter, $N_{eq,a}$ (see Eq. (2)), corresponding to each considered orientation. By maximizing the fatigue parameter (see Fig. 11 **(a)**), the crack nucleation orientation is evaluated for each loading condition. Such values are listed in Table 3, where it can be observed that they correspond to cracks nucleating toward the centre of the contact zone, in agreement with the experimental ones. However, it can be highlighted that the present methodology seems to fail in estimating the crack nucleation orientation when the rolling phenomenon is neglected, since the results do not fall within the range of the experimental standard deviation (see Table 2).

N_{cal} is listed in Table 3 for each examined loading condition. Moreover, such values are compared to the corresponding experimental ones in Fig. 12(a), where the dashed lines represent the scatter band equal to 2. It is possible to observe that only one slightly non-conservative estimation has been obtained (i.e., that related to the test No. T3), and all the results were inside the scatter band 3. Therefore, a quite good correlation in terms of fatigue life has been obtained between the experimental findings and the results estimated by employing the present methodology.

In order to further check the accuracy of the present methodology, the root mean square error [48] is computed as:

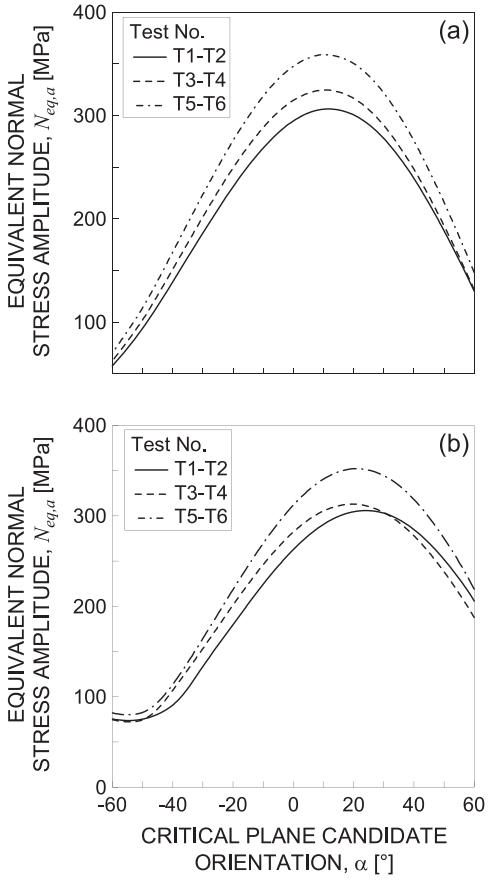

Fig. 11. Amplitude of the equivalent normal stress, $N_{eq,a}$, acting on the critical plane candidate as a function of the critical plane candidate orientation, α, computed with the FE model: (a) neglecting rolling and (b) incorporating rolling.

Table 3
Crack nucleation orientations, α_{cal} and α^R_{cal}, and fatigue lives, N_{cal} and N^R_{cal}, obtained with the present methodology, by neglecting and incorporating the rolling of the pads, respectively.

Test No.	α_{cal}[°]	α^R_{cal}[°]	N_{cal}[cycles]	N_{cal}/N_{exp}	N^R_{cal}[cycles]	N^R_{cal}/N_{exp}
T1	12	24	67948	0.77	85629	0.97
T2				0.76		0.96
T3	11	20	48653	1.02	76421	1.60
T4				0.94		1.48
T5	11	21	22130	0.44	31567	0.63
T6				0.56		0.81

$$T_{RMS} = 10^{\sqrt{\frac{\sum_{j=1}^{6} Log^2(N_{cal}/N_{exp})_j}{6}}} \quad (5)$$

In the present case, a T_{RMS} value equal to 1.55 has been found, thus confirming the fairly good accuracy of the results obtained.

5.2. Results obtained incorporating rolling

In this case, the hot-spot, H^R_{cal}, is found at $x^R_{cal} = 0.94mm$, $1.16mm$, and $1.10mm$ for the simulations of the tests No. T1-T2, T3-T4, and T5-T6, respectively. In particular, it can be noted that the hot-spot is found inside the slip zone for all the simulations performed, in agreement with the experimental results. However, it has to be noted that the crack nucleation locations predicted by neglecting the rolling are closer to the experimental observations. More precisely, although with both FE models the hot-spot is found more towards the centre of the contact zone with respect to the experimental one, the horizontal coordinate computed when the rolling is incorporated in the numerical simulation, x^R_{cal}, is about $0.3mm$ lower than the corresponding one obtained neglecting this phenomenon, x_{cal}, for each loading condition. Such a finding is related to the fact that the maximum value of σ_1 achieved in the fretting cycle is located more towards the centre of the contact zone when rolling is considered, than in the case of neglecting it. This can be noted by comparing respectively Fig. 7(a), (b) and (c) to Fig. 13(a), (b) and (c), where the maximum principal stress, σ_1, along the contact surface is plotted for 14 different equally-spaced time steps between the load steps No. 4 and 6 (see Fig. 5(b)), by considering the loading conditions of the tests No. T1-T2, T3-T4 and T5-T6, respectively.

Subsequently, the crack nucleation orientation, α_{cal}, is determined for each loading condition analysed. The values of N_a and N_m, computed

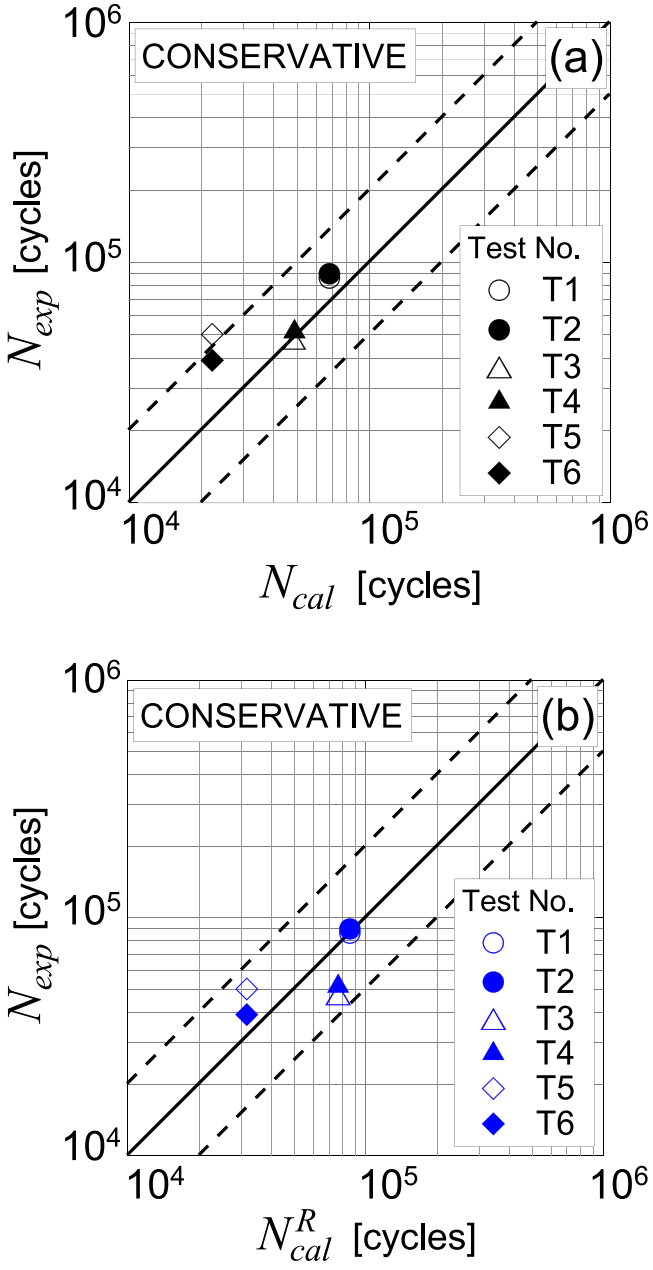

Fig. 12. Experimental fatigue lives against the corresponding values calculated with the presented methodology and exploiting the FE model: (a) neglecting and (b) incorporating the rolling of the pads.

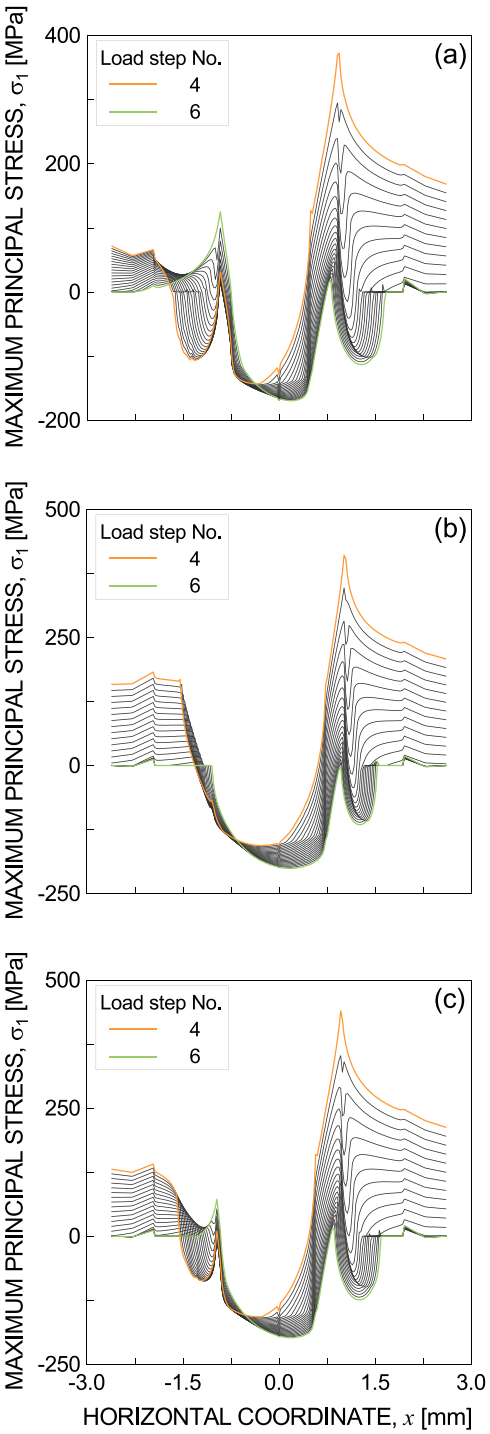

Fig. 13. Maximum principal stress, σ_1, along the contact surface, obtained with the FE model neglecting rolling at different time steps between the load steps No. 4 and 6 (see Fig. 5(b)), for the loading conditions of the tests No.: (a) T1-T2, (b) T3-T4, and (c) T5-T6.

along each α – oriented segment (see Fig. 6), from the hot-spot (point 1) up to $2d$ (point 10), are plotted in Figs. 14–16 for the loading conditions of the tests No. T1-T2, T3-T4 and T5-T6, respectively.

Then, the crack nucleation orientation, that is the orientation that maximizes the fatigue parameter, $N_{eq,a}$ (see Fig. 11 (b)), computed according to Eq. (2) by employing the average values, $\bar{N}_a$ and $\bar{N}_m$, of the above stress components, is evaluated for each loading condition. Such values are listed in Table 3, where it can be observed that they agree with the experimental ones, since both of them indicate cracks

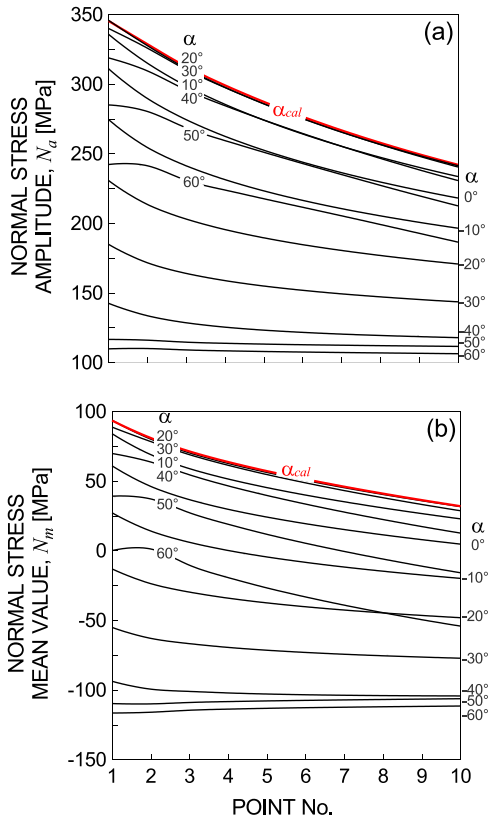

Fig. 14. Tests No. T1-T2: (a) amplitude and (b) mean value of the normal stress component computed in equally-spaced points along each α – oriented segment, from the hot-spot (point 1) up to $2d$ (point 10), by incorporating the rolling of the pad.

nucleating toward the centre of the contact. Moreover, it is possible to highlight that all the estimations are in good agreement with the experimental findings, falling within the range of the experimental standard deviations (see Table 2). Accordingly, it can be stated that the present methodology is able to correctly estimate the crack nucleation orientation when the rolling phenomenon is considered. Moreover, it can be highlighted that the estimations provided by the present methodology in terms of crack nucleation orientation are more accurate when the rolling phenomenon is considered with respect to the case of neglecting it.

Furthermore, N_{cal}^{R} is listed in Table 3 for each examined loading condition. Moreover, in Fig. 12(b) such values are compared to the corresponding experimental ones. It is possible to observe that all the results fall into scatter band 2, with 67% of conservative estimations. Therefore, a good correlation in terms of fatigue life has been obtained between the experimental findings and the results estimated by employing the present methodology.

The T_{RMS}^{R} value is equal to 1.39, thus confirming the high level of accuracy of the results obtained. Moreover, it is interesting to observe that such a value is 10% lower than the corresponding T_{RMS} value computed neglecting the rolling (see Sub-Section 5.1). Therefore, taking the rolling into account when applying the present methodology improves the fatigue life estimations with respect to the case of neglecting such a phenomenon.

6. Conclusions

In the present paper, the fretting fatigue assessment of an aluminium alloy has been performed through a methodology based on both a multiaxial fatigue criterion and the CDM, in conjunction with FE numerical simulations. Both a FE model that neglects the rolling of the pads

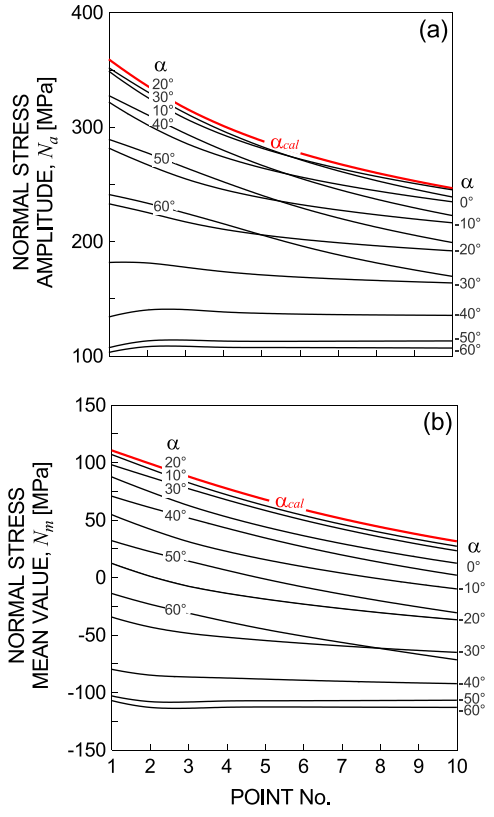

Fig. 15. Tests No. T3-T4: (a) amplitude and (b) mean value of the normal stress component computed in equally-spaced points along each α – oriented segment, from the hot-spot (point 1) up to 2*d* (point 10), by incorporating the rolling of the pad.

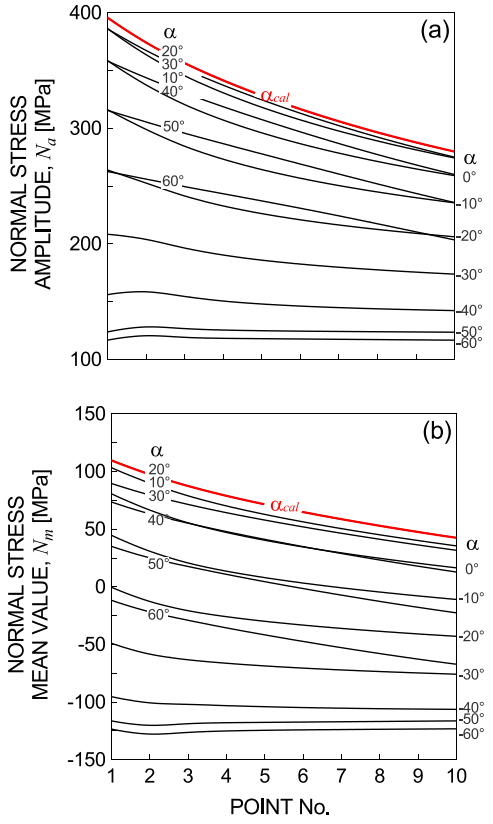

Fig. 16. Tests No. T5-T6: (a) amplitude and (b) mean value of the normal stress component computed in equally-spaced points along each α – oriented segment, from the hot-spot (point 1) up to 2*d* (point 10), by incorporating the rolling of the pad.

and a FE model that incorporates its effect have been exploited in order to find out the stress field within the specimens.

The estimated crack nucleation locations have been found inside the slip zone for all the simulations performed, in agreement with the experimental results. Moreover, the crack nucleation locations have been found more towards the centre of the contact zone by employing both the above models with respect to the experimental observations, although the experimental crack nucleation locations have been better predicted when the rolling of the pads is neglected.

The estimated crack nucleation orientations are in accordance to the experimental ones by employing both the above FE models. Moreover, when the rolling phenomenon is considered, the present methodology provides better results in terms of crack nucleation orientation with respect to the case of neglecting the rolling, with all the orientations falling within the range of the experimental standard deviations.

The estimated lifetime obtained by neglecting the rolling of the pads were less accurate, although more conservative, than those obtained by incorporating such a phenomenon. The root mean square error was equal to 1.55 and 1.39 by employing the numerical model neglecting or incorporating the rolling, respectively.

Therefore, it can be highlighted that a remarkable level of accuracy has been attained by both neglecting and considering the rolling of the pads, although in the latter case even more satisfactory results have been obtained.

Certificate of originality

This is to certify, that the research paper submitted is an outcome of our independent and original work.

Declaration of Competing Interest

The authors declare that they have no known competing financial interests or personal relationships that could have appeared to influence the work reported in this paper.

Data Availability

Data will be made available on request.

References

[1] Juoksukangas J, Lehtovaara A, Mäntylä A. Experimental and numerical investigation of fretting fatigue behavior in bolted joints. Tribology Int 2016;103:440–8.
[2] Moraes JFC, Rao1 HM, Jordon JB, Barkey ME. High cycle fatigue mechanisms of aluminum self-piercing riveted joints. Fatigue and Fracture of Engineering. Mater Struct 2018;41:57–70.
[3] Erena D, Vázquez Valeo J, Navarro C, Domínguez J. New fatigue device for testing cables: design and results. Fatigue Fract Eng Mater Struct 2019;42(8):1826–37. https://doi.org/10.1111/ffe.13022.
[4] Vantadori S, Vázquez Valeo J, Zanichelli A. Fretting fatigue and shot peening: a multiaxial fatigue criterion including residual stress relaxation. Tribology Int 2020;151:106537. 10.1016/j.triboint. 2020.106537.
[5] Zanichelli A, Ronchei C, Scorza D, Vantadori S. Influence of hot-spot on crack path and lifetime estimation of fretting-affected steel components. Theor Appl Fract Mech 2022;121:103467. https://doi.org/10.1016/j.tafmec.2022.103467.
[6] Soria SR, Claramonte S, Yawny A. Determination of the fretting maps on Incoloy 800 steam generator tubes against AISI 420 steel. Tribology Int 2023;180:108242. https://doi.org/10.1016/j.triboint.2023.108242.
[7] Wang J, Lei Y-J, Li Z-Y, Li H-J, Ren Q-Y, Jiao Y-J, et al. Effect of contact misalignment on fretting wear behavior between fuel cladding and Zr-4 grid. Tribology Int 2023;181:108299. https://doi.org/10.1016/j.triboint.2023.108299.
[8] Said J, Fouvry S, Cailletaud G, Yang C, Hafid F. Shear driven crack arrest investigation under compressive state: prediction of fretting fatigue failure of aluminium strands. Int J Fatigue 2020;136:105589.

[9] Carpinteri A, Vantadori S, Zanichelli A. Lifetime estimation of mechanical assemblies under constant amplitude fretting fatigue loading. Fatigue Fract Eng Mater Struct 2019;42(9):1927–36. https://doi.org/10.1111/ffe.13043.
[10] Hertz H. Miscellaneous Paper by Heinrich Hertz. New York: Macmillan & Co; 1896.
[11] Cattaneo C. Sul contatto di due corpi elastici: distribuzione locale degli sforzi. Rendiconti dell'Accademia Nazionale dei Lincei, 1938; 27, 6: 342–348.
[12] Mindlin RD. Compliance of elastic bodies in contact. ASME J Appl Mech 1949;16: 259–68.
[13] Nowell D, Hills DA. Mechanics of fretting fatigue tests. Int J Mech Sci 1987;29: 355–65.
[14] Vázquez J, Navarro C, Domínguez J. Analytical solution for a cylindrical contact with reverse slip. J Strain Anal Eng Des 2013;48(3):189–97. https://doi.org/10.1177/0309324712466977.
[15] Jager J. A new principle in contact mechanics. J Tribology 1998;120(4):677–84.
[16] Davies M, Barber J, Hills D. Energy dissipation in a frictional incomplete contact with varying normal load. Int J Mech Sci 2012;55(1):13–21.
[17] Williams ML. Stress singularities resulting from various boundary conditions in angular corners of plates in extension. J Appl Mech 1952;4(19):526–34.
[18] Bogy DB. Edge-bonded dissimilar orthogonal elastic wedges under normal and shear loading. J Appl Mech 1968;35(3):460.
[19] Dini D, Hills DA. Bounded asymptotic solutions for incomplete contacts in partial slip. Int J Solids Struct 2004;41(24–25):7049–62.
[20] Fleury R, Hills D, Ramesh R, Barber J. Incomplete contacts in partial slip subject to varying normal and shear loading, and their representation by asymptotes. J Mech Phys Solids 2017;99:178–91.
[21] Erena D, Vázquez J, Navarro C, Domínguez J. Numerical analysis of toroidal voids as stress relievers in shrink-fitted shafts. Tribology Int 2020;143:105996. https://doi.org/10.1016/j.triboint.2019.105996.
[22] Pinto AL, Cardoso RA, Talemi R, Araújo JA. Fretting fatigue under variable amplitude loading considering partial and gross slip regimes: Numerical analysis. Tribology Int 2020;146:106199. https://doi.org/10.1016/j.triboint.2020.106199.
[23] Erena D, Martín V, Vázquez J, Navarro C. Influence of the rolling of contact pads on crack initiation in fretting fatigue tests. Int J Fatigue 2022;163:107087. https://doi.org/10.1016/j.ijfatigue.2022.107087.
[24] Li H, Zhao Y, Jiang J, Wang H, He J, Liu J, et al. Effect of frequency on the fatigue performance of bolted joints under axial excitation. Tribology Int 2022;176: 107933. https://doi.org/10.1016/j.triboint.2022.107933.
[25] Vantadori S, Abbasi F, Zanichelli A, Leonetti D, Pucillo GP, Hossein Majzoobi G. Influence of normal load frequency on fretting fatigue behaviour by a critical plane-based approach. Int J Fatigue 2022;158:106724. https://doi.org/10.1016/j.ijfatigue.2022.106724.
[26] Vantadori S, Vázquez Valeo J, Zanichelli A, Carpinteri A, Luciano R. Structural integrity of shot peened Ti6Al4V specimens under fretting fatigue. Int J Fract 2022; 234(1–2):45–55. DOI: 10.1007/s10704-021-00523-0.
[27] Vázquez J, Erena D, Navarro C, Domínguez J. 3D contact effects in fretting fatigue tests. Theor Appl Fract Mech 2022;118:103260. https://doi.org/10.1016/j.tafmec.2022.103260.
[28] Shu Y, Liu Z, Yang G. Finite element simulation of fretting wear on railway axle press-fit specimens. Tribology Int 2023;178:108024. https://doi.org/10.1016/j.triboint.2022.108024.
[29] Zhao B, Sun Q, Zhao R, Yang Y, Sun K, Mu X. Mass-eccentricity nonlinear evolution mechanism of combined rotor in fretting slip process. Tribology Int 2023;179: 108195. https://doi.org/10.1016/j.triboint.2022.108195.
[30] Madge JJ, Leen SB, Shipway PH. The critical role of fretting wear in the analysis of fretting fatigue. Wear 2007;263(1–6):542–51.
[31] Gandiolle C, Fouvry S. Experimental analysis and modeling of the crack arrest condition under severe plastic fretting fatigue conditions. Procedia Eng 2013;66: 783–92.
[32] Moës N, Dolbow J, Belytschko T. A finite element method for crack growth without remeshing. Int J Numer Methods Eng 1999;46(1):131–50.
[33] Giner E, Sukumar N, Fuenmayor FJ, Vercher A. Singularity enrichment for complete sliding contact using the partition of unity finite element method. Int J Numer Methods Eng 2008;76(9):1402–18.
[34] Cardoso RA, Néron D, Pommier S, Araújo JA. An enrichment-based approach for the simulation of fretting problems. Comput Mech 2018;62(6):1529–42.
[35] Vantadori S, Zanichelli A. Fretting-fatigue analysis of shot-peened aluminium and titanium test specimens. Fatigue Fract Eng Mater Struct 2021;44(2):397–409.
[36] Zanichelli A. Advanced methodology for fretting fatigue assessment of metallic structural components. ESIS Publishing House, 2021.
[37] Zanichelli A, Vantadori S. Shot-peened fretting fatigue components: endurance strength and fatigue life assessment. Mater Des Process Commun 2021;3(4):e196.
[38] Vantadori S, Zanichelli A, Ronchei C, Scorza D, Carpinteri A. Investigation on crack nucleation location in fretting-affected Al 7050-T7451 alloy. Int J Fatigue 2022; 163:107016. https://doi.org/10.1016/j.ijfatigue.2022.107016.
[39] Carpinteri A, Ronchei C, Scorza D, Vantadori S. Critical plane orientation influence on multiaxial high-cycle fatigue assessment. Phys Mesomech 2015;18(4):348–54.
[40] Vantadori S, Carpinteri A, Luciano R, Ronchei C, Scorza D, Zanichelli A, et al. Crack initiation and life estimation for 316 and 430 stainless steel specimens by means of a critical plane approach. Int J Fatigue 2020;138:105677.
[41] Vantadori S, Ronchei C, Scorza D, Zanichelli A, Carpinteri A. Fatigue behaviour assessment of ductile cast iron smooth specimens. Int J Fatigue 2021;152:106459.
[42] Zanichelli A, Ronchei C, Scorza D, Vantadori S. Fatigue lifetime of both plain and notched specimens made of additively manufactured AISI 316L. J Mater Res Technol 2022;21:2532–46. https://doi.org/10.1016/j.jmrt.2022.10.068.
[43] Araújo JA, Almeida GMJ, Ferreira JLA, da Silva CRM, Castro FC. Early cracking orientation under high stress gradients: the fretting. Int J Fatigue 2017;100: 302–11.
[44] Araújo JA, Castro FC, Matos IM, Cardoso RA. Life prediction in multiaxial high cycle fretting fatigue. Int J Fatigue 2020;134:105504.
[45] Erena D, Martín V, Vázquez J, Navarro C. Rolling effect in fretting fatigue test at the crack initiation stage. Procedia Struct Integr 2022;39:104–10.
[46] Martín V, Vázquez J, Navarro C, Domínguez J. Fretting-fatigue analysis of shotpeened Al 7075–T651 test specimens. Metals 2019;9(5):586. https://doi.org/10.3390/met9050586.
[47] Vázquez J, Navarro C, Domínguez J. Experimental results in fretting fatigue with shot and laser peened Al 7075-T651 specimens. Int J Fatigue 2012;40:143–53.
[48] Vantadori S, Carpinteri A, Luciano R, Ronchei C, Scorza D, Zanichelli A. Mean stress effect on fatigue life estimation for Inconel 718 alloy. Int J Fatigue 2020;133: 105391.